Modified optical absorption of molecules on metallic nanoparticles at sub-monolayer coverage

Brendan L. Darby, Baptiste Auguié, Matthias Meyer, Andres E. Pantoja and Eric C. Le Ru*

Enhanced optical absorption of molecules in the vicinity of metallic nanostructures is key to a number of surface-enhanced spectroscopies and of great general interest to the fields of plasmonics and nano-optics. However, experimental access to this absorbance has long proven elusive. Here, we present direct measurements of the surface absorbance of dye molecules adsorbed onto silver nanospheres and, crucially, at sub-monolayer concentrations where dye–dye interactions become negligible. With a large detuning from the plasmon resonance, distinct shifts and broadening of the molecular resonances reveal the intrinsic properties of the dye in contact with the metal colloid, in contrast to the often studied strong-coupling regime where the optical properties of the dye molecules cannot be isolated. The observation of these shifts together with the ability to routinely measure them has broad implications in the interpretation of experiments involving resonant molecules on metallic surfaces, such as surface-enhanced spectroscopies and many aspects of molecular plasmonics.

Over the last two decades, the optical properties of metallic nanoparticles of various sizes and shapes[1] have been exploited in numerous contexts: for sub-wavelength light manipulation, as nano-antennas[2] or as building blocks for meta-materials[3]; for ultrasensitive spectroscopy, such as surface-enhanced fluorescence[4,5] (SEF) and Raman spectroscopy[6–8] (SERS); or as sensors[9–11]. More recent applications are emerging, leveraging this understanding of plasmonic optical properties and relying on the rigorous modelling offered by electromagnetic theory: we can cite, for example, the development of new types of chiroptical spectroscopies[12], the enhancement of photochemical reactions on surfaces[13–16], enhanced light emission in light-emitting diodes (LEDs)[17] or improved photovoltaics[18–20]. Many of these existing and emerging applications are underpinned by the fact that the optical (electronic) absorption of molecules on the surface of metallic nanoparticles is enhanced. However, spectral changes induced by molecular adsorption are often ignored because of the experimental challenge of measuring surface absorbance spectra on nanoparticles, despite early attempts more than 30 years ago[21].

This problem is not addressed directly in the great number of recent studies devoted to the topic of strong coupling between plasmons and molecules[22–36]. In this regime, the plasmon–molecule interaction is evidenced by a typical anti-crossing of the two resonances as a function of detuning[25,33], but in such a strongly interacting system the molecular response cannot be isolated. Moreover, in such studies the dye concentration is often large (typically monolayer coverage and above) to maximize dye–plasmon interactions. Dye–dye interactions cannot therefore be neglected and are expected to induce resonance shifts of the dye layer independently of any plasmonic effects. In fact, many studies specifically work with *J*-aggregates rather than isolated dyes[22,25–27,31,33]. As a result, the intrinsic effect (chemical and/or electromagnetic) of the nanoparticle on an isolated adsorbed molecule cannot be elucidated. To this end, we will show that it is necessary to measure the absorbance of the dye when the dye and plasmon resonances are detuned (to avoid dye–plasmon interaction effects) and at low surface coverage (to avoid dye–dye interaction effects). This low surface coverage poses a significant experimental challenge because the dye absorbance is then very small, and is overwhelmed by the large optical response (absorption and scattering) of the nanoparticles.

Here, we propose to measure nanoparticle/dye solutions inside an integrating sphere to obtain the modified absorbance spectra of the commonly used chromophores Rhodamine 700, Rhodamine 6G, Nile Blue and Crystal Violet adsorbed onto spherical silver nanoparticles in solution, at dye concentrations of the order of only 10 nM. This approach enables the first direct experimental observation of the surface absorbance of dyes on nanoparticles in a regime where dye–dye and dye–plasmon resonance interactions are negligible. The observation of noticeable changes in the absorption spectrum of several common dyes clearly demonstrates that spectral shifts are the norm rather than the exception and therefore crucial to quantitative interpretation of many SERS, SEF or molecular plasmonics experiments involving dyes.

Predictions from electromagnetic theory

Figure 1 presents a general description of the problem, using Mie theory to model the optical response of silver colloids and a standard isotropic effective medium[22,25,27,30,31,33,35,36] for the thin coating layer of adsorbed dyes (see Methods and Supplementary Section I). This simple shell model allows us to illustrate the principle of the experimental technique and highlight a number of difficulties to be overcome in practice. Figure 1a considers the optical properties of a colloidal solution of silver nanospheres (30 nm radius) in water. For a colloid concentration of 8 pM, as used in this work, the peak extinction corresponds to an optical density (OD) of 0.85 cm^{-1}. In comparison, the peak extinction of a typical chromophore has an OD of only 10^{-3} cm^{-1} at a concentration of 10 nM. This dye concentration corresponds to sub-monolayer coverage on the colloid surface. Assuming 100% adsorption for simplicity, this translates to ~1,200 dyes per colloid, or 0.1 dye nm^{-2}. This is therefore low enough to ensure negligible interaction between dyes and is also in the typical range for surface-enhanced spectroscopy experiments, but remains much larger than for single-molecule conditions[10].

The MacDiarmid Institute for Advanced Materials and Nanotechnology, School of Chemical and Physical Sciences, Victoria University of Wellington, PO Box 600, Wellington 6140, New Zealand. *e-mail: eric.leru@vuw.ac.nz
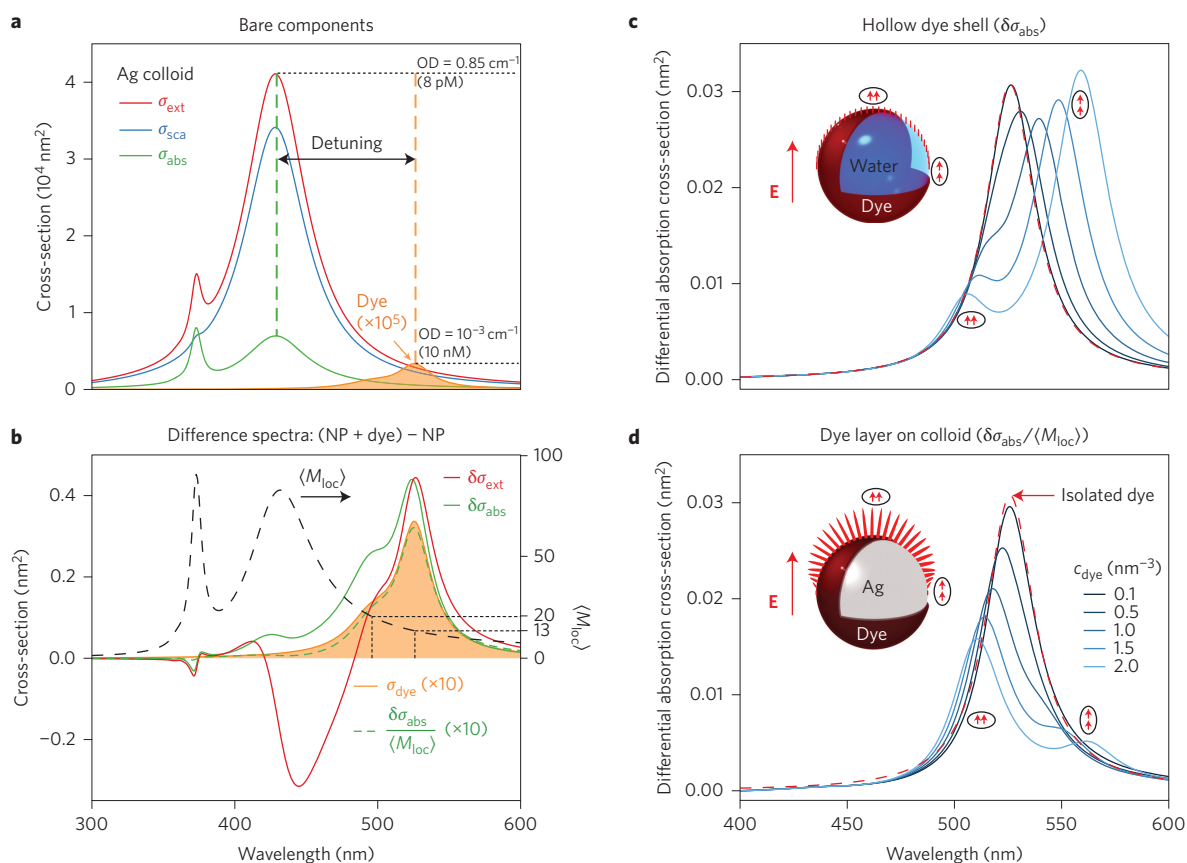
Figure 1 | Mie theory simulations of dye-coated spheres. a, Extinction (red), absorption (green) and scattering (blue) cross-sections for a silver nanosphere (30 nm radius) in water, and the absorption cross-section of a typical dye (orange). Peak optical densities (ODs) are indicated for concentrations of 8 pM silver colloids and 10 nM dye. **b**, Difference spectra obtained by subtracting the response of the bare sphere shown in **a** from the same colloid coated with a 1 nm dye shell (concentration, 0.1 nm^{-3}). The corrected differential absorbance $\delta\sigma_{abs}(\lambda)/\langle M_{loc}(\lambda)\rangle$, where $\langle M_{loc}\rangle$ is the surface-averaged field intensity enhancement factor (black dashed line), closely matches the reference dye absorbance. **c,d**, Differential absorption spectra as a function of dye concentration (from 0.1 to 2.0 nm^{-3}) in the shell (normalized by $\langle M_{loc}\rangle$ in **d**) and reference dye spectrum (red dashed line). The fictitious hollow shell with the nanoparticle replaced by water (**c**) is used as a toy model to understand the case of a dye layer on a silver sphere (**d**). Insets: polarization ellipses of the local electric field (at 530 nm).

A natural approach to retrieve the absorbance spectrum of the adsorbed dye would then consist of measuring the UV–vis extinction spectrum for the mixture, and subtracting a reference taken as the bare colloids (with no adsorbed dyes). If the dye and plasmon resonance coincided, it would be difficult to disentangle them, but because the detuning between the dye and plasmon resonances is chosen to be relatively large (100 nm), one could expect to isolate a meaningful absorbance for the dye. However, as shown in Fig. 1b, this naive approach does not work: the predicted difference spectrum obtained from extinction measurements departs substantially from the absorbance spectrum of the adsorbed dye, showing a negative difference within the tail of the plasmon resonance, strongly distorting the lineshape around 500 nm. This is a consequence of the minute shift of the plasmon resonance induced by the dye layer and is comparable in magnitude to the dye absorbance itself. This unavoidable effect is largely alleviated by considering the differential absorbance $\delta\sigma_{abs}(\lambda)$, which results in a spectrum similar to that of the original dye. The nanoparticle absorbance is approximately six times smaller than extinction, thus allowing easier extraction of the dye contribution within the otherwise overwhelming nanoparticle scattering response. A closer look at Fig. 1b nevertheless shows that $\delta\sigma_{abs}(\lambda)$ is not exactly the same as that of the bare dye, in particular in the relative intensity of the main and vibronic peaks. This is attributed to the wavelength dependence of the plasmonic enhancement, which for absorption is

characterized by the surface-averaged local field intensity enhancement factor[6] $\langle M_{loc}(\lambda)\rangle$. This effect is secondary and cannot cause a significant resonance shift, but can nevertheless be accounted for: the corrected differential absorbance spectrum $\delta\sigma_{abs}(\lambda)/\langle M_{loc}(\lambda)\rangle$ then resembles very closely the true surface absorbance of the dye, as seen in Fig. 1b. The same conclusions are obtained for a polydisperse solution of nanospheres as used in our experiments (Supplementary Section II).

This discussion has so far focused on a low dye concentration, but in many of the previous studies dye concentrations have instead been large, typically at or beyond monolayer coverage. Figure 1c,d illustrates how dye–dye interactions may then interfere with the measurement of the surface absorbance of the adsorbed dye. As the dye concentration increases, the electromagnetic (EM) interaction between dyes needs to be included in the effective medium properties of the coating layer, which we describe via the Clausius–Mossotti equation (see Methods). To disentangle the effect of the nanoparticles from the intrinsic dye–dye interactions we consider a fictitious dye-coated water nanosphere in Fig. 1c as a toy model, and compare it to the same shell on a silver sphere. In the latter case, the differential absorbance is corrected for the plasmonic enhancement as discussed earlier. Below concentrations of 0.1 dye nm^{-3} in the shell, local-field (Clausius–Mossotti) corrections are negligible and the differential absorbance spectra in Fig. 1c, d, closely match the spectrum of the free dye in solution (dashed red

lines). As the dye concentration increases, the dye resonance splits into two resonances, as predicted from the standard exciton model[37]: the blueshifted resonance is associated with the side-by-side dipolar interaction between dyes, while the redshifted one corresponds to head-to-tail induced dipoles. Both resonances are excited in a spherical shell as shown in the surface-field diagram in Fig. 1c. The same types of interaction are expected for Ag–dye core–shell structures, but the electric field is then mostly perpendicular to the surface (Fig. 1d, inset). Thus for an isotropic dye layer on a metal nanoparticle, the blueshifted (side-by-side) resonance will be favoured. These predictions highlight the importance of dye–dye interaction effects in dye layers.

We conclude this preliminary discussion with a summary of our findings for the determination of the surface absorbance of dye molecules adsorbed on silver colloids. First, differential absorbance measurements should be preferred over extinction. Second, a large detuning from the plasmon resonance simplifies the analysis, allowing direct access to the modified dye absorbance, which is only scaled by the plasmonic enhancement factor $\langle M_{\mathrm{loc}}(\lambda) \rangle$. Finally, low dye concentrations should be used to limit the effect of dye–dye interactions. This combination of factors results in challenging experiments and requires pushing the limit of detection of currently available instruments with new developments.

Results

To tackle this problem we used a UV–vis absorption set-up with the sample centrally located inside an integrating sphere (Fig. 2a; see Methods and Supplementary Section III for details). This particular configuration has only been used on rare occasions and mostly for the characterization of seawater[38–40]. The integrating sphere eliminates the influence of scattering, with a direct measurement of absorbance, rather than extinction. In our configuration, it also increases the effective path length to ~2.4 cm (Supplementary Section II). With appropriate precautions (see Methods) we achieved accurate referencing of the dye–nanoparticle solution absorbance spectrum against an identical nanoparticle-only solution, with ~1×10^{-4} relative accuracy. These developments allowed us to measure the extremely small differential absorbance spectra required for this study, with a lower limit down to an OD of ~1×10^{-4} cm^{-1}.

Figure 2 highlights some of the observations that are made possible by this novel approach. Figure 2b shows the differential absorbance spectra of the dye Rhodamine 700 (RH700) adsorbed on silver nanoparticles at three different concentrations (6, 12 and 24 nM). The reference absorbance spectrum of this dye in water (shown in grey) exhibits a main resonance at 642 nm with a vibronic shoulder at 590 nm. Figure 2b clearly demonstrates the ability of our approach to measure the surface absorbance of dyes on nanoparticles at very low concentrations, down to 6 nM here. The most dramatic observation is the clear redshift of the surface absorption spectrum by ~20 nm, with the main resonance now at 664 nm. As explained earlier, this cannot be due to the interaction with the plasmon resonance (the dye and plasmon resonances are detuned by more than 200 nm). This shift cannot be attributed to dye–dye interactions either. The effect of the dye–dye interaction is in fact visible in the concentration dependence and results in a (very small) blueshift of the resonances together with a change in relative intensity between the two peaks at 12 and 24 nM. These two features are also predicted by the theoretical electromagnetic model (shown as dashed lines). The observed redshift at the lowest concentration must therefore be an intrinsic feature of the adsorbed dye.

The measured spectrum at 6 nM remains affected by the plasmonic enhancement factor $\langle M_{\mathrm{loc}}(\lambda) \rangle$, which is easily accounted for using the effective shell model. By fitting the experimental surface absorbance spectrum measured at 6 nM to this model, we can

therefore deduce the modified intrinsic surface polarizability of RH700 (see Supplementary Section IV for details), as shown in Fig. 2c. However, the oscillator strength for this modified transition appeared at first ~5.3 times smaller than that of the original spectrum. Although we cannot exclude this possibility, it is more likely that the oscillator strength is unchanged and that the magnitude of the actual absorption enhancement is smaller than predicted (by the same factor, ~5.3). In fact, electromagnetic theory predicts that for a silver sphere with a radius of 30 nm, the average absorption should be enhanced by a factor of $\langle M_{\mathrm{loc}} \rangle = 6.4$ at 664 nm, but this implicitly assumes an isotropic polarizable dipole. Most dyes, however (including RH700), have a strongly uniaxial transition dipole moment along the π-conjugated backbone of the molecule. Because the local electric field is primarily perpendicular to the metal surface (with only $\langle M_{\mathrm{loc}}^{\parallel} \rangle = 0.17$ for the parallel component at 664 nm), the observed enhancement in absorption will be strongly dependent on the preferential orientation of the adsorbed dye. This effect is similar to surface-selection rules in surface-enhanced spectroscopies[7,41]. The observed reduced absorption enhancement can therefore be attributed to an adsorption orientation preferentially flat (or at a small angle) on the surface, which is expected for dyes with such an aromatic backbone. In this context, the assumption of a conserved oscillator strength appears the most natural, and the deduced modified absorbance is shown in Fig. 2c along with that of RH700 in water. This 'surface absorbance' represents the absorption spectrum of the isolated adsorbed dye in solution.

This measured modified absorbance can then be used to predict within the Mie–shell model the concentration dependence as shown in Fig. 2b (dashed lines). The shell thickness L_{D}, which is an 'effective' monolayer thickness in this model[42], was adjusted to $L_{\mathrm{D}} = 0.6$ nm to reproduce the observed evolution of the relative intensity of the two peaks. The predicted spectra are in close agreement with the experimental results, barring the scaling factor of 5.3 previously discussed. One may nevertheless notice that the theory predicts a larger blueshift at high concentrations than observed experimentally. This discrepancy is consistent with the expectation that the dye is preferentially adsorbed flat. As discussed in Fig. 1d, the blueshift is related to side-by-side interactions between induced dipoles perpendicular to the metal surface, and would be much less prevalent for flat adsorption. The general agreement between theory and experiment in Fig. 2b provides strong evidence that the observed changes in relative peak intensities can be attributed to dye–dye interactions and that these effects can remain important even at very low concentrations, here down to ~10 nM, in a regime where many surface-enhanced spectroscopy experiments are carried out.

We have also extended this study to other chromophores commonly used in surface-enhanced spectroscopies, namely Crystal Violet (CV), Nile Blue (NB) and Rhodamine 6G (RH6G), adsorbed onto the same silver colloids. Those complementary results are summarized in Fig. 3. Of the four dyes, CV exhibits the most noticeable change in absorption, with a ~90 nm blueshift to 500 nm from its main absorption peak in water at 590 nm. Such a dramatic spectral shift suggests a major chemical change for the adsorbed species. CV is known to be sensitive to pH[43], because the number of protonated nitrogen groups strongly affects its resonance. We speculate that chemical binding to silver may have a similar effect here. In contrast to CV, NB shows no major resonance shift, which may be interpreted as a weaker interaction with the surface through physisorption. A broadening of the absorbance spectrum at long wavelengths is also observed and could be attributed to inhomogeneous broadening as a result of varying surface–dye interactions from one molecule to another. Finally, the observations for RH6G are comparable to those of RH700, except that even lower concentrations (down to 2.5 nM) are necessary to reach the regime where dye–dye interactions become negligible. In fact, at 10 nM,
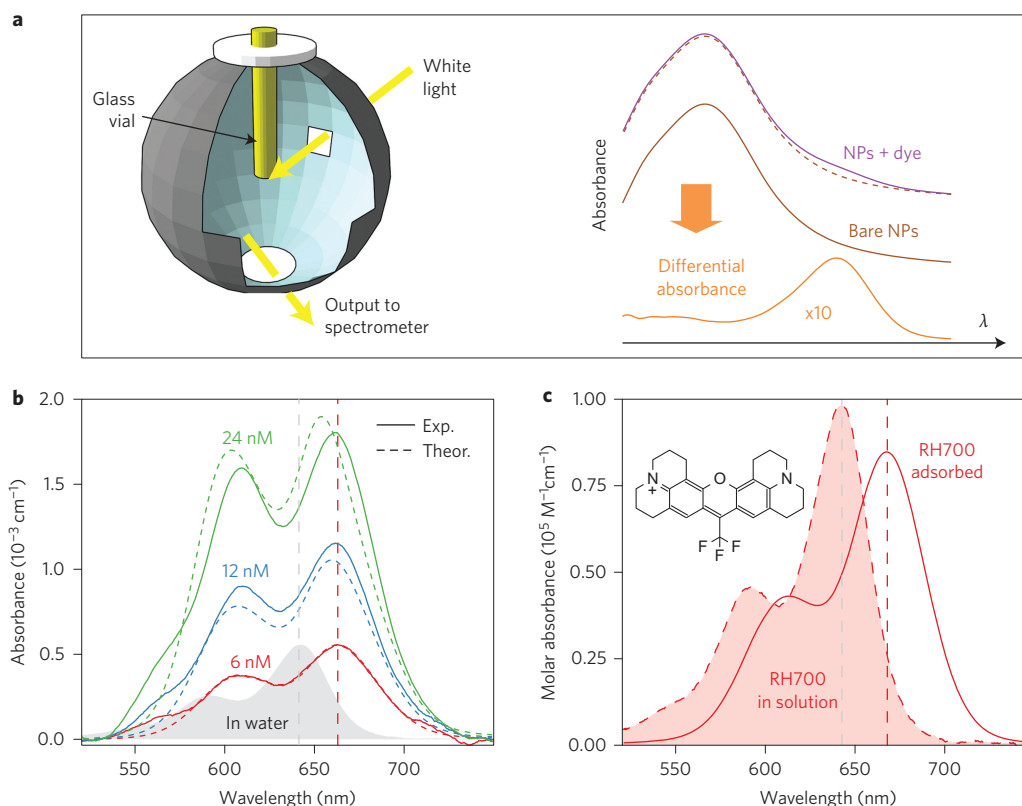
Figure 2 | Differential absorbance measurements. a, Schematic of set-up and principle of measurement of the differential absorbance of dyes on nanoparticles. **b**, Measured (solid lines) and predicted (dashed lines) differential absorbance spectra of RH700 at concentrations of 6, 12 and 24 nM on silver nanospheres (30 nm radius, 8 pM). Those spectra are redshifted by ~20 nm compared with the reference RH700 spectrum in water (shown in grey). Note an intensity scaling factor of ~5.3 is necessary to quantitatively match experiments and theory (see discussion in the text). The modified surface polarizability of RH700 was modelled as a double-Voigt-type resonance, with the same oscillator strength as bare RH700 and parameters adjusted to fit the experimental surface absorbance spectrum measured at 6 nM. The effective thickness of the shell was adjusted to $L_D = 0.6$ nm. **c**, Comparison between the deduced absorption spectra of adsorbed RH700 and the reference bare RH700 (inset: chemical formula of RH700).

the spectrum is clearly strongly modified by these effects (Supplementary Section V). This may be because dimer formation is more likely, as suggested in previous studies[24], but further work is necessary to fully elucidate this aspect. The most likely explanation for the observed redshift for RH700 and RH6G is that the metallic surface perturbs the electronic structure of the molecules—as would any dielectric environment—as predicted from density functional theory (DFT) calculations[44].

In terms of absolute spectrum intensity, NB exhibits an absorption enhancement factor comparable to that of RH700, that is, on the order of 1.2 assuming conserved oscillator strength and a much smaller than predicted isotropic enhancement of $\langle M_{loc} \rangle \approx 6.4$ at 650 nm. This is consistent with a flat adsorption geometry, as independently confirmed for NB in air on gold surfaces[41]. CV and RH6G exhibit larger apparent absorption enhancements on the order of 4, the largest (assuming a preserved oscillator strength) being for RH6G at ~4.4. This smaller discrepancy with the predicted isotropic enhancement of $\langle M_{loc} \rangle \approx 12$ at 540 nm suggests that RH6G does not adsorb with its electronic transition dipole exactly parallel to the metal surface like RH700 and NB. This is consistent with its non-planar geometry, due to an additional ring oriented perpendicular to the main backbone. Further extensions of the EM model to anisotropic and inhomogeneous dye layers will be necessary to confirm the importance of orientational effects.

Discussion and conclusion
Our proposed technique, based on the measurement of the differential absorbance of a sample inside an integrating sphere, provides a unique approach to experimentally access the surface absorbance spectra of chromophores adsorbed on nanoparticles. It could also be directly applied to the study of non-metallic nanoparticles and using an ultraviolet light source, to molecules other than dyes.

Our results clearly highlight the great potential of this technique for ultrasensitive absorbance measurements in the presence of strongly scattering media, such as solutions of metallic colloids. The ability to measure the surface absorbance of dyes on metallic nanoparticles paves the way for more detailed studies of both dye–surface and dye–dye interactions. Recent related works in this area[45,46] have been limited to adsorbed molecules on flat metal films and exposed to air, using polarization- and/or angle-dependent transmittance/reflectance spectroscopy. In such studies, it is extremely challenging to reliably control the molecular surface coverage/concentration because of the solution-to-surface transfer step. Moreover, the ambient medium can have a strong effect on the absorbance of dyes, and the results obtained in air cannot be easily compared to the reference measured in water. Our method mitigates both of these issues by working in solution and can reliably reach sub-monolayer concentrations.

Two important conclusions stand out from this study, which we expect to have many implications. First, modifications of the intrinsic dye polarizability upon adsorption on metallic nanoparticles appear to be the norm rather than the exception. Second, further modifications arising from dye–dye interactions remain important even at relatively low surface coverage, in fact in a range relevant to many experiments. Both of these effects should be carefully considered for many experiments involving
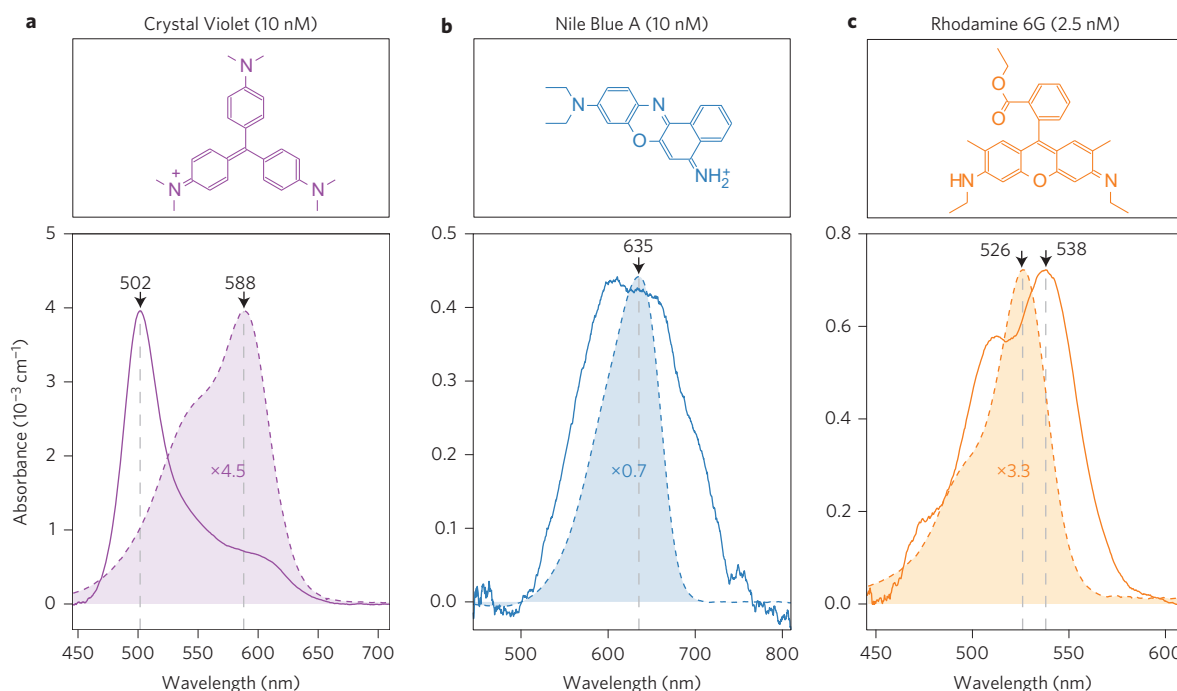
Figure 3 | Differential absorbance spectra of common dyes adsorbed on silver nanoparticles. a, Crystal Violet. **b**, Nile Blue A. **c**, Rhodamine 6G. The colloid concentration is 8 pM. The dye concentrations are low enough (10, 10 and 2.5 nM, respectively) to avoid any effects from dye–dye interactions. Dashed lines are the reference spectra in water that would be measured at the same concentration, scaled for easier visualization. The oscillator strength enhancements in each case are 3.4, 1.2 and 4.4, respectively. The dye chemical formulae are reproduced at the top of each panel for reference.

dyes adsorbed on the surface of metallic nanoparticles, notably molecular plasmonics (strong coupling, plexcitonics) and SERS, SEF and other surface-enhanced spectroscopies. As an example, the experimental determination of SERS enhancement factors[47] typically assumes that the polarizability of the probe molecule is not modified upon adsorption. In view of our results, this assumption should clearly be revisited for experiments in resonance or pre-resonance conditions, with implications for the debate over the 'chemical enhancement' mechanism[48]. Although a small shift as observed for RH6G may not have any significant effect, the consequences of the large shift observed for CV should be major and for example be clearly evident in wavelength-dependent measurements of SERS enhancement factors. Similarly, in the context of molecular plasmonics, most studies are interpreted in terms of coupling between dye and plasmon resonances, where the dye (or J-aggregate) spectrum is assumed to be unchanged in contact with the metal. While this may be the case for some molecules, our results suggest that such an assumption should be carefully checked on a case-by-case basis and that dye–dye interactions and/or absorbance modification may play a major role in interpreting experimental results.

Beyond those direct consequences, we anticipate that our experimental findings will spark a fruitful discussion on the interpretation of the observed spectral changes for different molecules. New experimental access to such a regime of molecule–metal interaction with a non-obtrusive optical technique will undoubtedly encourage further tests and refinements of DFT predictions of the resonance of dye–metal complexes. It will also offer a deeper insight into the subtle interplay between electromagnetic effects, including selection rules linked to preferential orientation on the surface and those of a more chemical nature attributed to changes in the electronic configuration of a molecule physisorbed or chemisorbed onto a surface. A refined understanding of these mechanisms will have a profound impact on the interpretation and further development of surface-enhanced Raman scattering, chiroptical or fluorescence spectroscopies.

Methods

Methods and any associated references are available in the online version of the paper.

References

1. Grzelczak, M., Perez-Juste, J., Mulvaney, P. & Liz-Marzán, L. M. Shape control in gold nanoparticle synthesis. *Chem. Soc. Rev.* **37,** 1783–1791 (2008).
2. Schuller, J. A. *et al.* Plasmonics for extreme light concentration and manipulation. *Nature Mater.* **9,** 193–204 (2010).
3. Hess, O. *et al.* Active nanoplasmonic metamaterials. *Nature Mater.* **11,** 573–584 (2012).
4. Kühn, S., Håkanson, U., Rogobete, L. & Sandoghdar, V. Enhancement of single-molecule fluorescence using a gold nanoparticle as an optical nanoantenna. *Phys. Rev. Lett.* **97,** 017402 (2006).
5. Le Ru, E. C. *et al.* Mechanisms of spectral profile modification in surface-enhanced fluorescence. *J. Phys. Chem. C* **111,** 16076–16079 (2007).
6. Le Ru, E. C. & Etchegoin, P. G. *Principles of Surface Enhanced Raman Spectroscopy and Related Plasmonic Effects* (Elsevier, 2009).
7. Moskovits, M. Surface-enhanced spectroscopy. *Rev. Mod. Phys.* **57,** 783–826 (1985).
8. Aroca, R. *Surface-Enhanced Vibrational Spectroscopy* (Wiley, 2006).
9. Barhoumi, A., Zhang, D., Tamand, F. & Halas, N. J. Surface-enhanced Raman spectroscopy of DNA. *J. Am. Chem. Soc.* **130,** 5523–5529 (2008).
10. Le Ru, E. C. *et al.* A scheme for detecting every single target molecule with surface-enhanced Raman spectroscopy. *Nano Lett.* **11,** 5013–5019 (2011).
11. Brolo, A. G. Plasmonics for future biosensors. *Nature Photon.* **6,** 709–713 (2012).
12. Govorov, A. O., Fan, Z., Hernandez, P., Slocik, J. M. & Naik, R. R. Theory of circular dichroism of nanomaterials comprising chiral molecules and nanocrystals: plasmon enhancement, dipole interactions, and dielectric effects. *Nano Lett.* **10,** 1374–1382 (2010).
13. Xu, S., Shan, J., Shi, W., Liu, L. & Xu, L. Modifying photoisomerization efficiency by metallic nanostructures. *Opt. Express* **19,** 12336–12341 (2011).
14. Kleinman, S. L., Frontiera, R. R., Henry, A.-I., Dieringer, J. A. & Van Duyne, R. P. Creating, characterizing, and controlling chemistry with SERS hot spots. *Phys. Chem. Chem. Phys.* **15,** 21–36 (2013).
15. Galloway, C. M., Artur, C., Grand, J. & Le Ru, E. C. Photobleaching of fluorophores on the surface of nanoantennas. *J. Phys. Chem. C* **118,** 28820–28830 (2014).

16. Linic, S., Christopher, P. & Ingram, D. B. Plasmonic-metal nanostructures for efficient conversion of solar to chemical energy. *Nature Mater.* **10,** 911–921 (2011).

17. Lozano, G. *et al.* Plasmonics for solid-state lighting: enhanced excitation and directional emission of highly efficient light sources. *Light Sci. Appl.* **2,** e66 (2013).

18. Atwater, H. A. & Polman, A. Plasmonics for improved photovoltaic devices. *Nature Mater.* **9,** 205–213 (2010).

19. Mubeen, S. *et al.* On the plasmonic photovoltaic. *ACS Nano* **8,** 6066–6073 (2014).

20. Sheldon, M. T., van de Groep, J., Brown, A. M., Polman, A. & Atwater, H. A. Plasmoelectric potentials in metal nanostructures. *Science* **346,** 828–831 (2014).

21. Craighead, H. G. & Glass, A. Optical absorption of small metal particles with adsorbed dye coats. *Opt. Lett.* **6,** 248–250 (1981).

22. Wiederrecht, G. P., Wurtz, G. A. & Hranisavljevic, J. Coherent coupling of molecular excitons to electronic polarizations of noble metal nanoparticles. *Nano Lett.* **4,** 2121–2125 (2004).

23. Haes, A. J., Zou, S., Zhao, J., Schatz, G. C. & Van Duyne, R. P. Localized surface plasmon resonance spectroscopy near molecular resonances. *J. Am. Chem. Soc.* **128,** 10905–10914 (2006).

24. Zhao, J. *et al.* Interaction of plasmon and molecular resonances for Rhodamine 6G adsorbed on silver nanoparticles. *J. Am. Chem. Soc.* **129,** 7647–7656 (2007).

25. Fofang, N. T. *et al.* Plexcitonic nanoparticles: plasmon–exciton coupling in nanoshell–J-aggregate complexes. *Nano Lett.* **8,** 3481–3487 (2008).

26. Ni, W. *et al.* Effects of dyes, gold nanocrystals, pH, and metal ions on plasmonic and molecular resonance coupling. *J. Am. Chem. Soc.* **132,** 4806–4814 (2010).

27. Ni, W., Ambjörnsson, T., Apell, S. P., Chen, H. & Wang, J. Observing plasmonic–molecular resonance coupling on single gold nanorods. *Nano Lett.* **10,** 77–84 (2010).

28. Davis, T. J., Gómez, D. E. & Vernon, K. C. Interaction of molecules with localized surface plasmons in metallic nanoparticles. *Phys. Rev. B* **81,** 045432 (2010).

29. Valmorra, F. *et al.* Strong coupling between surface plasmon polariton and laser dye Rhodamine 800. *Appl. Phys. Lett.* **99,** 051110 (2011).

30. Chen, H., Shao, L., Woo, K. C., Wang, J. & Lin, H.-Q. Plasmonic–molecular resonance coupling: plasmonic splitting versus energy transfer. *J. Phys. Chem. C* **116,** 14088–14095 (2012).

31. Zengin, G. *et al.* Approaching the strong coupling limit in single plasmonic nanorods interacting with J-aggregates. *Sci. Rep.* **3,** 3074 (2013).

32. Fang, Y., Blinn, K., Li, X., Weng, G. & Liu, M. Strong coupling between Rhodamine 6G and localized surface plasmon resonance of immobile Ag nanoclusters fabricated by direct current sputtering. *Appl. Phys. Lett.* **102,** 143112 (2013).

33. Schlather, A. E., Large, N., Urban, A. S., Nordlander, P. & Halas, N. J. Near-field mediated plexcitonic coupling and giant Rabi splitting in individual metallic dimers. *Nano Lett.* **13,** 3281–3286 (2013).

34. Faucheaux, J. A., Fu, J. & Jain, P. K. Unified theoretical framework for realizing diverse regimes of strong coupling between plasmons and electronic transitions. *J. Phys. Chem. C* **118,** 2710–2717 (2014).

35. Antosiewicz, T. J., Apell, S. P. & Shegai, T. Plasmon–exciton interactions in a core–shell geometry: from enhanced absorption to strong coupling. *ACS Photon.* **1,** 454–463 (2014).

36. Cacciola, A., Di Stefano, O., Stassi, R., Saija, R. & Savasta, S. Ultrastrong coupling of plasmons and excitons in a nanoshell. *ACS Nano* **8,** 11483–11492 (2014).

37. Kasha, M. Energy transfer mechanisms and the molecular exciton model for molecular aggregates. *Radiat. Res.* **20,** 55–70 (1963).

38. Nelson, N. B. & Prézelin, B. B. Calibration of an integrating sphere for determining the absorption coefficient of scattering suspensions. *Appl. Opt.* **32,** 6710–6717 (1993).

39. Babin, M. & Stramski, D. Light absorption by aquatic particles in the near-IR spectral region. *Limnol. Oceanogr.* **47,** 911–915 (2002).

40. Gaigalas, A. K., He, H.-J. & Wang, L. Measurement of absorption and scattering with an integrating sphere detector: application to microalgae. *J. Res. Natl Inst. Stand. Technol.* **114,** 69–81 (2009).

41. Le Ru, E. C. *et al.* Experimental demonstration of surface selection rules for SERS on flat metallic surfaces. *Chem. Commun.* **47,** 3903–3905 (2011).

42. Dignam, M. J. & Moskovits, M. Optical properties of sub-monolayer molecular films. *J. Chem. Soc. Faraday Trans. II* **69,** 56–64 (1973).

43. Angeloni, L., Smulevich, G. & Marzocchi, M. Resonance Raman spectrum of Crystal Violet. *J. Raman Spectrosc.* **8,** 305–310 (1979).

44. Morton, S. M. & Jensen, L. A discrete interaction model/quantum mechanical method for describing response properties of molecules adsorbed on metal nanoparticles. *J. Chem. Phys.* **133,** 074103 (2010).

45. Forker, R., Gruenewald, M. & Fritz, T. Optical differential reflectance spectroscopy on thin molecular films. *Annu. Rep. Prog. Chem. Sect. C Phys. Chem.* **108,** 34–68 (2012).

46. Dietze, D. R. & Mathies, R. A. Molecular orientation and optical properties of 3,3′-diethylthiatricarbocyanine iodide adsorbed to gold surfaces: consequences for surface-enhanced resonance Raman spectroscopy. *J. Phys. Chem. C* **119,** 9980–9987 (2015).

47. Le Ru, E. C. & Etchegoin, P. G. Quantifying SERS enhancements. *MRS Bull.* **38,** 631–640 (2013).

48. Moskovits, M. Persistent misconceptions regarding SERS. *Phys. Chem. Chem. Phys.* **15,** 5301–5311 (2013).

Acknowledgements

Author contributions

B.L.D. and E.C.L.R. designed the original ideas presented in this work and built the experimental set-up with A.E.P. B.L.D. carried out most of the experiments. M.M. optimized various aspects of the experimental set-up, carried out extensive calibration, and performed the DFT calculations. B.A., B.L.D. and E.C.L.R. developed and performed the electromagnetic theory and calculations. The manuscript was jointly written by B.L.D., B.A. and E.C.L.R. All authors discussed the results and the manuscript.

Additional information

Supplementary information is available in the online version of the paper. Reprints and permissions information is available online at www.nature.com/reprints. Correspondence and requests for materials should be addressed to E.C.L.R.

Competing financial interests

The authors declare no competing financial interests.

Methods

Materials. All dyes and nanoparticles were used as purchased and diluted appropriately. Rhodamine 700, Rhodamine 6G, Nile Blue and Crystal Violet were purchased from Sigma Aldrich in powder form and mixed with ultrapure MilliQ water to the desired stock concentration (in the range 10–100 µM). Stock solutions of 60-nm-diameter citrate-covered silver nanospheres in water (particle concentration 1.9×10^{10} ml^{-1}, equivalent to 32 pM) were purchased from Nanocomposix and stored sealed in a fridge at 4 °C.

Absorbance measurements. A modified Ocean Optics ISP-80 integrating sphere was used for all absorbance measurements. Volumes of 2 ml of solution were pipetted into a cylindrical glass tube (67.5 mm long, 7 mm external diameter, wall thickness 1 mm) and were carefully inserted into the integrating sphere through a port in the north pole. A custom holder was used to ensure reproducibility of the tube position and orientation. White-light illumination was provided by a 100 W halogen lamp and delivered to the sphere's equatorial port via a ThorLabs 1,000 µm 0.22 NA optical fibre. Collection was made via a similar optical fibre (910 µm, 0.22 NA) inserted into a custom-drilled detection port in the bottom of the sphere and coupled to an Ocean Optics USB-2000+ spectrometer with 100 µm entrance slits and a detection range of 200–850 nm. Spectra were acquired as the average of 10,000 individual 1 ms spectra (giving an effective total exposure of 10 s) and corrected with identically acquired dark spectra. Care was taken to avoid the nonlinear region of the detector, keeping counts near one-quarter of the charge-coupled device pixel well-depth.

Absorbance spectra were then obtained from the standard relation $A(\lambda) = -\log_{10}(I_S(\lambda)/I_R(\lambda))$, where I_S and I_R are the detected intensities of the sample and reference. For the differential absorbance of adsorbed dyes on nanoparticles, the reference is the same nanoparticle solution with no dyes. All differential absorbance spectra were then corrected by the effective path length, $L_{sphere} = 2.4$ cm, to yield the optical density in cm^{-1}. L_{sphere} was determined by measuring the absorbance of Eosin B and Nile Blue in water inside the sphere and comparing to the absorbance measured in a standard UV–vis set-up. Moreover, because Eosin B is negatively charged, it does not adsorb to the silver nanoparticles and its absorbance spectrum inside the sphere is unchanged when measured in colloidal solution. This confirms that the strong scattering of the colloidal solution has no effect on the differential absorbance spectra. See Supplementary Section III for further details.

Sample preparation. All colloid samples were prepared according to the guidelines outlined in ref. 49. Each set of measurements required a reference solution. Reference samples were prepared by first mixing 500 µl of silver colloid solution with 500 µl of 2 mM KCl to displace the citrate capping layer (without inducing aggregation[49]). This solution was then mixed with 1 ml of MilliQ water and the resulting 2 ml (with a final colloid concentration of 8 pM) was pipetted into a cylindrical glass tube. The same procedure was performed for dye–colloid samples but replacing the water in the final dilution by twice the desired concentration of dye. For each concentration series, the same vial was used to ensure exactly the same vial geometry for all measurements, and concentrations were tested going from reference (no dye) to the highest dye concentration sequentially. Vials were cleaned with aqua regia before measuring and were rinsed thoroughly with water and ethanol after measuring each sample.

Note that this method relies on the assumption that the addition of dyes (which are charged) to colloids does not induce any intrinsic change in the colloid, in particular aggregation. Were aggregation present in the dye–colloid sample,

referencing with bare colloids would no longer be valid. For the dye concentrations and the type of colloids used here, aggregation is not expected and would be evident in the appearance of a longer-wavelength absorption peak associated with nanoparticle aggregates, which is not present in the spectra measured.

Theory. Theoretical predictions of the optical properties of the dye layer were carried out using an isotropic shell model as used in most recent studies of strong coupling in molecular plasmonics[22,25,27,30,31,33,35,36]. This consists of solving the electromagnetic scattering problem for a metallic nanosphere covered by a thin spherical shell (of thickness L_D) with an effective dielectric function that models the dye response. Note that L_D can here be viewed as an effective thickness, only loosely connected to the physical size of the dye molecule; that is, it is an adjustable parameter (whose meaning is defined more precisely in ref. 42). To study the dye concentration dependence, it is necessary to start from the polarizability of the individual dyes and account for local field corrections using the Clausius–Mossotti (CM) relation in the two-dimensional dense dye layer, as one would do in a bulk three-dimensional phase. This has been studied in the past[42] and we adapted it to the case where the dyes are embedded in a medium, here water with a dielectric constant $\varepsilon_M = 1.77$. The effective dielectric function of the dye layer is then

$$\varepsilon_{dye} = \frac{1 + \frac{2}{3}(\tilde{\alpha}_M + \tilde{\alpha}_D)}{1 - \frac{1}{3}(\tilde{\alpha}_M + \tilde{\alpha}_D)} \qquad (1)$$

where $\tilde{\alpha}_M$ and $\tilde{\alpha}_D$ are the normalized bare polarizabilities of the solvent and dye molecules. The former is simply deduced from the standard CM equation in a pure phase

$$\tilde{\alpha}_M = 3\frac{\varepsilon_M - 1}{\varepsilon_M + 2}(\approx 0.61) \qquad (2)$$

The latter depends directly on the density of dyes in the shell layer, via the concentration of dyes c_D (note that this is related to the number of dyes per unit area μ_D by $c_D \approx \mu_D/L_D$)

$$\tilde{\alpha}_D(\omega) = c_D\frac{\alpha_D}{\varepsilon_0} \qquad (3)$$

The bare polarizability $\alpha_D(\omega)$ can be deduced from the measured optical absorbance of the dye up to a constant related to the static polarizability, which is calculated by DFT (see Supplementary Section I for details).

The electromagnetic problem is solved using Mie theory for multilayered spheres using standard codes[50]. The dielectric function of silver is taken from the analytical fit in ref. 6. $\langle M_{loc}(\lambda)\rangle$ is calculated for the nanoparticle-only model, by taking the average of the field intensity enhancement factor on the spherical surface in the middle of the thin shell.

References

49. Darby, B. L. & Le Ru, E. C. Competition between molecular adsorption and diffusion: dramatic consequences for SERS in colloidal solutions. *J. Am. Chem. Soc.* **136**, 10965–10973 (2014).
50. Le Ru, E. C. & Etchegoin, P. G. SERS and plasmonics codes (SPlaC); http://www.vuw.ac.nz/raman/book/codes.aspx